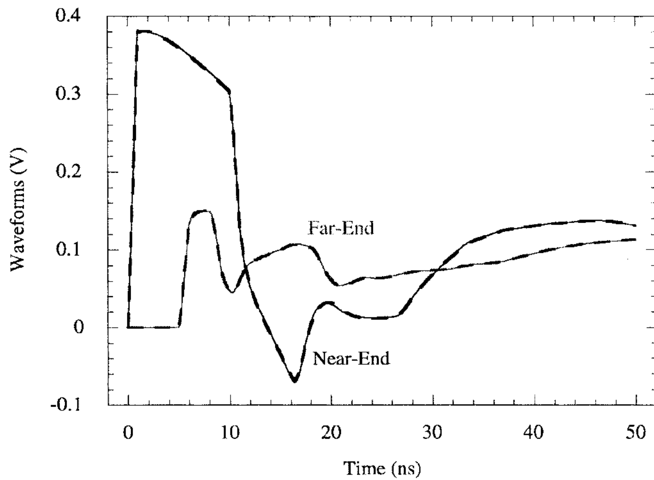

Fig. 3. Transient waveforms at conductor 3 of the four-conductor frequency-dependent parabolically tapered line of [2]. Thin continuous curves show the results obtained with the open-loop model and thick dashed curves show those for the open-loop internal-reflection model.

models installed in a modified nodal approach (MNA)-based circuit simulator. The results are in excellent agreement with the analytical solutions in [2, p. 12, Fig. 4(a) and (b)]. Seventh-order real-pole approximation was used for the open-loop model, and a 17th-order complex-pole approximation was used for the open-loop internal-reflection model.

The run-time comparisons for circuits of various sizes and types can be found in [1]. The run-time data in [1] were obtained with the open-loop nonuniform line model.

IV. Conclusions

This paper presented the application of the transmission-line simulation method [1] to nonuniform lines. Two novel nonuniform line models were introduced.

The open-loop model results in the simplest aperiodic responses (similar to those for uniform lines), which can be accurately represented by a few samples and a low-order approximation with only real poles. The model, however, does not guarantee stability of the line characterization.

The open-loop internal-reflection model provides the simplest stable characterization, which is, however, more complex than the open-loop characterization and requires a higher order approximation with complex poles.

References

[1] D. B. Kuznetsov and J. E. Schutt-Ainé, "Optimal transient simulation of transmission lines," *IEEE Trans. Circuits Syst. I,* vol. 43, pp. 111–121, Feb. 1996.

[2] F.-Y. Chang, "Transient simulation of frequency-dependent nonuniform coupled lossy transmission lines," *IEEE Trans. Comp., Packag., Manufact. Technol.,* vol. 17, pp. 3–14, Feb. 1994.

[3] ——, "Transient simulation of nonuniform coupled lossy transmission lines characterized with frequency-dependent parameters, Part I: Waveform relaxation analysis," *IEEE Trans. Circuits Syst. I,* vol. 39, pp. 582–603, Aug. 1992.

[4] ——, "Transient simulation of nonuniform coupled lossy transmission lines characterized with frequency-dependent parameters, Part II: Discrete-time analysis," *IEEE Trans. Circuits Syst. I,* vol. 39, pp. 907–927, Nov. 1992.

[5] M. T. Correia de Barrosand and M. E. Almeida, "Computation of electromagnetic transients on nonuniform transmission lines," *IEEE Trans. Power Delivery,* vol. 11, pp. 1082–1091, Apr. 1996.

[6] J.-F. Mao and Z.-F. Li, "Waveform relaxation solution of the $ABCD$ matrices of nonuniform transmission lines for transient analysis," *IEEE Trans. Computer-Aided Design,* vol. 13, pp. 1409–1412, Nov. 1994.

[7] A. S. Al Fuhaid, "s-domain analysis of electromagnetic transients on nonuniform lines," *IEEE Trans. Power Delivery,* vol. 5, pp. 2072–2083, Nov. 1990.

[8] S. He, "Frequency and time domain green function technique for nonuniform *LCRG* transmission lines with frequency-dependent parameters," *J. Electromagnetic Waves Applicat.,* vol. 7, pp. 31–38, 1993.

[9] C. Hsue and C. C. Hechtman, "Transient analysis of nonuniform, high-pass transmission lines," *IEEE Trans. Microwave Theory Tech.,* vol. 38, pp. 1023–1030, Aug. 1990.

[10] O. A. Palusinski and A. Lee, "Analysis of transients in nonuniform and uniform multiconductor transmission lines," *IEEE Trans. Microwave Theory Tech.,* vol. 37, pp. 127–138, Jan. 1989.

[11] Y.-C. Yang, J. A. Kong, and Q. Gu, "Time-domain perturbation analysis of nonuniformly coupled transmission lines," *IEEE Trans. Microwave Theory Tech.,* vol. MTT-33, pp. 1120–1130, Nov. 1985.

[12] J. L. Hill and D. Mathews, "Transient analysis of systems with exponential transmission lines," *IEEE Trans. Microwave Theory Tech.,* vol. MTT-25, pp. 777–783, Sept. 1977.

Micromachined Thermocouple Microwave Detector by Commercial CMOS Fabrication

Veljko Milanović, Michael Gaitan, and Mona E. Zaghloul

***Abstract*— This paper reports on the design and testing of a thermocouple microwave detector fabricated through a commercial CMOS foundry with an additional maskless etching procedure. The detector measures true rms power of signals in the frequency range from 50 MHz to 20 GHz, and input power range from −30 to +10 dBm. The device has linearity better than ±0.4% for input power versus output voltage over the 40-dB dynamic range. Measurements of the return loss, obtained using an automatic network analyzer, show acceptable input return loss of less than −20 dB over the entire frequency range. The sensitivity of the detector was measured to be (1.007 ±0.004) mV/mW.**

I. Introduction

Thermocouple-based power sensors have been one of the most widely used tools for microwave power detection [1]–[4].[1] These sensors employ a simple principle of conversion of electric power to thermal power, which is then indirectly measured.[2] A terminating resistor dissipates the microwave energy in the form of heat. The measurement of the temperature differential caused by the resistive

Manuscript received May 6, 1996; revised February 13, 1998. This work was supported by the Naval Command, Control and Ocean Surveillance Center, RDT&E DIV, San Diego, CA. The work of V. Milanović was supported by RF Microsystems, San Diego, CA.

V. Milanović and M. E. Zaghloul are with the Department of Electrical Engineering and Computer Science, The George Washington University, Washington, DC 20052 (e-mail: veljko@seas.gwu.edu) USA.

M. Gaitan is with the Semiconductor Electronics Division, National Institute of Standards and Technology, Gaithersburg, MD 20899 USA.

Publisher Item Identifier S 0018-9480(98)03154-8.

[1] Hewlett-Packard Co., "Fundamentals of RF and microwave power measurement," *Applicat. Note AN 64-1,* June 1978.

[2] J. R. Kinard, J. R. Hastings, T. E. Lipe, and C. B. Childers, *AC–DC Difference Calibration.* NIST Special Publication, vol. 250-27, May 1989.

0018–9480/98$10.00 © 1998 IEEE

heating provides an accurate measure of the true rms power absorbed by the terminating resistor. A thermocouple-based power sensor measures the heat generated in the terminating resistor by a thermopile that converts the temperature of the resistor to a dc voltage.[1] This method of measurement is conceptually independent of the input frequency and waveform, providing that the device components, especially the terminating resistors, are frequency independent.

Historically, standard CMOS technology cannot be used in microwave applications because of inefficiencies due to electromagnetic and thermal coupling of the devices. Currents induced in the silicon substrate due to electromagnetic coupling result in frequency-dependent losses [5]–[7]. Thermal coupling of a power-sensor terminating resistor to the substrate reduces its temperature response, making the sensor inefficient. Removing the substrate from directly beneath the resistor greatly reduces these inefficiencies while still allowing the monolithic integration of CMOS electronics [8].

Micromachining techniques are becoming increasingly popular in high-frequency applications [5]–[7]. At the same time, silicon micromachining techniques have also been applied to CMOS technology to make a variety of thermo–electro–mechanical structures [9]. Thermoelectric power sensors fabricated in CMOS technology have been reported for device structures operated below 1 GHz [1], [8]. In this paper, we report on a CMOS implementation of a thermoelectric microwave power detector, which operates efficiently up to 20 GHz. In the past [3], the thermocouple microwave detector structure was fabricated in a custom process where the dielectric and the conductive and resistive films are selected to optimize the device performance. However, digital and analog circuitry could not easily be monolithically integrated with the power sensor in the custom process.

Our implementation of this device structure in a commercial CMOS process results in the provision of monolithic integration of detection and output circuitry with the power sensor on a single chip. We have found that there is a tradeoff with slightly reduced accuracy because the conductive and resistive films are those that are available in the CMOS fabrication process: aluminum and polysilicon. However, the capability of fabricating this structure in CMOS technology could have a significant economic advantage as a low-cost microwave power sensor with integrated electronics where some loss in accuracy is acceptable. Our interest is to explore this issue and report on the performance of the device fabricated using a commercial CMOS foundry combined with subsequent post-CMOS fabrication silicon etch steps.

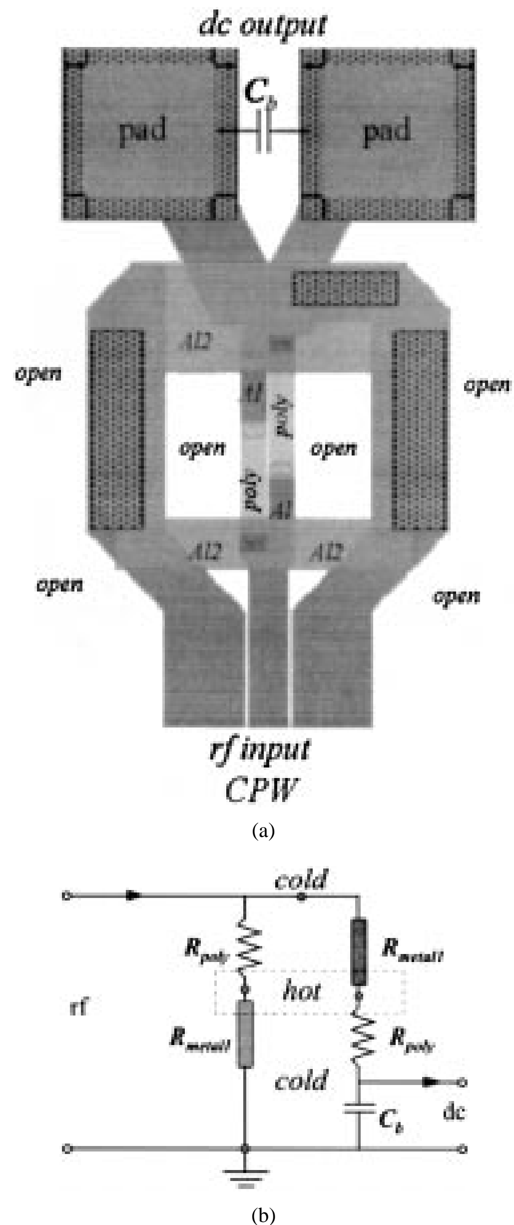

Fig. 1. MAGIC computer-aided design (CAD) layout of the sensor and equivalent circuit schematic.

II. Theory of Operation

The power sensor contains two identical thermocouples, electrically connected as shown in Fig. 1. Each thermocouple is an aluminum–polysilicon junction consisting of two resistors: $R_{\rm poly}$ and $R_{\rm metal1}$, as illustrated in Fig. 1. The combined series resistance of one thermocouple is $R_{\rm poly} + R_{\rm metal1} = 100\ \Omega$. The thermocouples are connected in series as far as the dc output is concerned. Looking from the microwave input, however, the two are in parallel, together forming a 50-Ω matching-impedance termination. This is accomplished by connecting the lower node of the left thermocouple (in Fig. 1) directly to ground, and connecting the lower node of the right thermocouple to "RF ground" through bypass capacitor C_b. Half the RF currents, therefore, flow through each thermocouple, heating them proportionally to the RF power at the input. The heat, however, is dissipated unevenly due to the layout, therefore forming the hot and cold junctions necessary to generate the dc voltage. Fig. 1 also shows the layout of the device. At the bottom are electrical probing pads for the RF input in a ground–signal–ground (GSG) configuration with 100-μm pitch. At the top of the structure are the probing pads for the dc output. The bypass capacitor C_b is externally connected to the pads. In the center are two thermocouples, surrounded with ground planes and cooler regions covered with second-layer metal ($Al2$). Both thermocouples form thermally isolated hot Al–poly junctions, adjacent to each other. These junctions are thermally and electromagnetically isolated by removing the substrate underneath and also removing the ground planes in direct vicinity. The cold junctions are formed because of the increased widths of the resistors, and also because of the proximity to the pads. The pads have large metal surfaces which efficiently guide the heat away into the surrounding substrate and air. A very important part of the layout are the *open* areas which expose the silicon substrate in designated areas for maskless etching. The *open* layer [10] specifies several passivation cuts, available in a standard CMOS process. The *open* areas are on both sides of the thermocouples, as shown in the layout in Fig. 1. As a result of such design, the fabricated IC's are readily micromachined without any additional photolithographical steps. The etching procedure is explained in Section III.

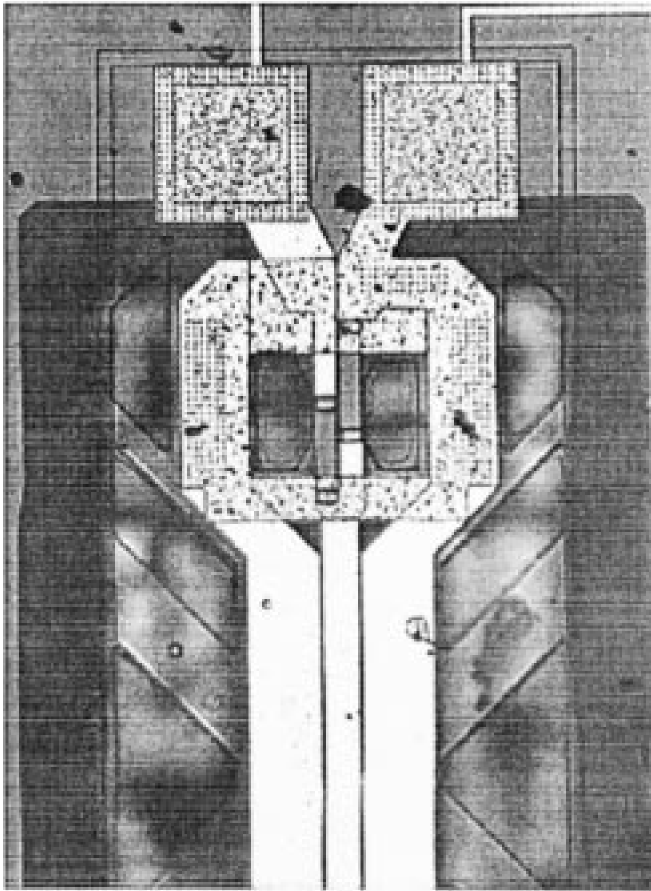

Fig. 2. Microphotograph of the fabricated device.

III. Fabrication and Measurement Setup

For characterization of the devices, a test chip was fabricated in a 2-μm CMOS n-well process through the MOSIS service [9]. The chip was subsequently etched in our laboratory. As shown in the layout in Fig. 1, the *open* areas are on both sides of the resistors of the conductive strips. Because there is no overlap of the *open* areas on the two sides, anisotropic etch would not suspend the resistors, but would instead form two separate etch pits on either side. For this reason, a hybrid etching method was used, explained in detail in [9]. In the first step, a gaseous isotropic etchant—xenondifloride—was used. After approximately 5 min (ten 30-s pulses), the pits that form on each side of the resistors connect beneath the structure, at which point anisotropic etching can be successfully applied. Chips are placed into an anisotropic etchant, called ethylene diamine–pyrocatechol water (EDP), and the exposed silicon is etched along its crystalline structure until an inverted pyramid pit is formed. Because of the relatively small size of the device, the EDP etch takes approximately 1 h at 92 °C. The resulting device is shown in the photograph in Fig. 2.

Measurements were performed at frequencies from 50 MHz up to 20 GHz using an automatic network analyzer, microwave probes for contacting the devices, and an accurate dc-voltage meter. To test the linearity of the device, signals with power from −30 to 10 dBm at 20 GHz were applied at the input, and output dc voltages were recorded. These measurements are shown in Fig. 3. The frequency dependence of the sensor was similarly recorded while sweeping the input frequency at constant power 0.0 dBm. The results are given in Fig. 4, showing linearity up to 20 GHz. Another important measurement is that of the input mismatch error of the device over the entire frequency range. The mismatch is determined from the measured s_{11} parameters of the RF input. The calibrated [10] reference plane for the measurement was the probe tip, and thus the results include the parasitic effects of the pads and underlying substrate. Nevertheless, the input mismatch error is below −20 dB over the entire frequency range, as shown in Fig. 5.

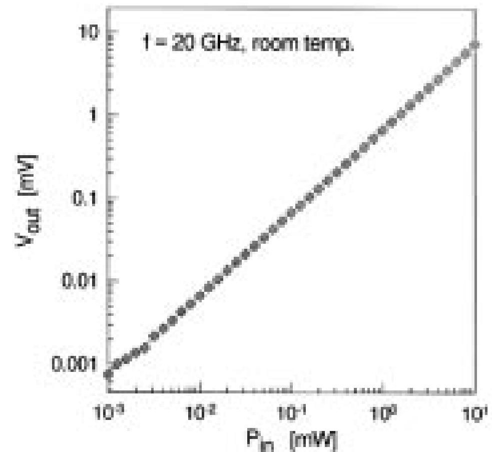

Fig. 3. Measured input power versus output voltage characteristics.

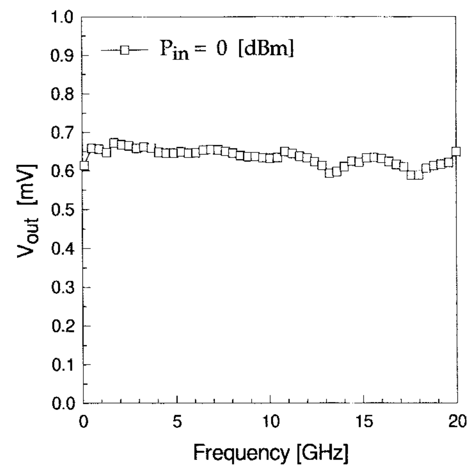

Fig. 4. Measured frequency versus output voltage characteristics.

IV. Discussion of the Results

Measurements have shown that the sensors have very good RF–dc linearity. As shown in Fig. 3, the input power to output voltage relationship is linear throughout the 40-dB input range. A ±0.4 linearity error was calculated from the measured data. The slope of the graph is (1.007 ± 0.004) mV/mW, which is an acceptable sensitivity for this type of device.[1] This sensitivity is due to the relatively high Seebeck coefficient of the aluminum–polysilicon thermocouples. Also, micromachining the substrate beneath the hot junctions results in a relatively high temperature gradient between the hot and cold contacts, further increasing the efficiency.

The frequency response is nearly flat to 20 GHz, as shown in Fig. 4. Although the resistors are suspended away from the silicon substrate, most of the structure remains over the substrate which creates very high losses in the microwave range. It is expected that the response would be less frequency dependent in a fully packaged device where the probing pads would be bonded and fully suspended as well. For on-wafer measurements, it becomes extremely difficult to perform

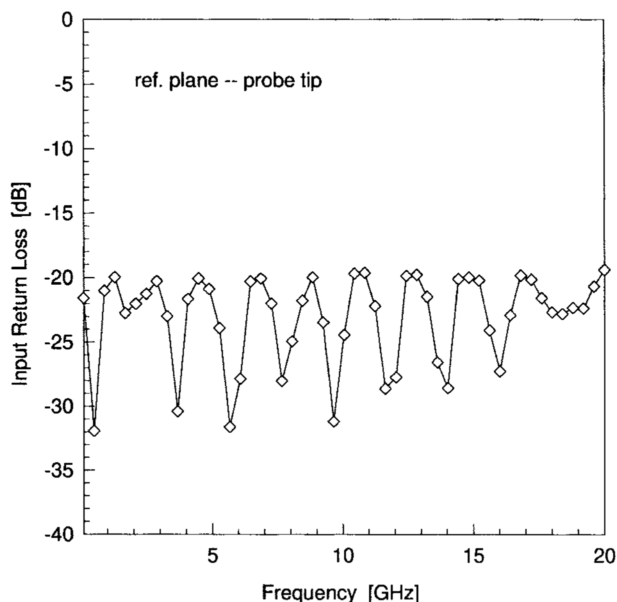

Fig. 5. Measured input return loss of the device.

accurate measurements when the contacts pads are partially or fully suspended.

The input mismatch measurements in Fig. 5 show acceptable mismatch error below -20 dB at all frequencies. As a result of the mismatch, the frequency dependence measurements from Fig. 4 have some further uncertainty, but can be neglected because of the small reflection coefficients. Also, as mentioned earlier, the s_{11} measurements were performed with probe tip calibration, including the parasitics in the probing pads and the underlying silicon. It is expected that the actual input return loss of the device without the pads would be even lower.

V. Conclusions

We presented a novel method for fabricating efficient microwave power sensors in CMOS technology, with an additional low-cost post-process step. The sensors are based on thermocouple measurement techniques. The devices show excellent linearity characteristics, and low return loss up to 20 GHz. The CMOS implementation gives the advantages of low cost and easy integration with CMOS circuits. The future goal is to integrate the devices with sensing and data conversion circuits on the same chip.

Acknowledgment

The authors wish to extend their thanks to RF Microsystems' Senior Scientist E. Bowen for technical discussions and reading of the manuscript. They would also like to acknowledge N. Tea and D. Berning for helpful discussions.

References

[1] D. Jaeggi and H. Baltes, "Thermoelectric AC power sensor by CMOS technology," *IEEE Electron Device Lett.,* vol. 13, pp. 366–368, July 1992.

[2] M. E. Goff and C. A. Barratt, "DC to 40 GHz MMIC power sensor," in *12th Annu. GaAs IC Symp. Tech. Dig.,* New Orleans, LA, Oct. 1990, pp. 105–108.

[3] L. A. Christel and K. Petersen, "A miniature microwave detector using advanced micromachining," in *IEEE Solid-State Sensors Actuator Workshop Tech. Dig.,* Hilton Head, SC, June 1992, pp. 144–147.

[4] P. Kopystynski, E. Obermeier, H. Delfs, and A. Loeser, "Silicon power microsensor with frequency range from DC to microwave," in *Int. Conf. Solid-State Sensors Actuators Dig.,* June 1991, pp. 623–626.

[5] V. Milanović, M. Gaitan, E. D. Bowen, and M. E. Zaghloul, "Micromachined microwave transmission lines in CMOS technology," *IEEE Trans. Microwave Theory Tech.,* vol. 45, pp. 630–635, May 1997.

[6] J. Y.-C. Chang, A. A. Abidi, and M. Gaitan, "Large suspended inductors on silicon and their use in a 2-μm CMOS RF amplifier," *IEEE Electron Device Lett.,* vol. 14, pp. 246–248, May 1993.

[7] L. P. B. Katehi, G. M. Rebeiz, T. M. Weller, R. F. Drayton, H. Cheng, and J. F. Whitaker, "Micromachined circuits for millimeter- and sub-millimeter-wave applications," *IEEE Antennas Propagat. Mag.,* vol. 35, pp. 9–17, Oct. 1993.

[8] M. Gaitan, J. R. Kinard, and D. X. Huang, "Performance of commercial CMOS foundry-compatible multijunction thermal converters," in *Proc. 7th Int. Conf. Solid-State Sensors Actuators,* Yokohama, Japan, June 1993, pp. 1012–1014.

[9] N. H. Tea, V. Milanović, C. A. Zincke, J. S. Suehle, M. Gaitan, M. E. Zaghloul, and J. Geist, "Hybrid post-processing etching for CMOS-compatible MEMS," *J. Microelectromech. Syst.,* vol. 6, pp. 363–372, Dec. 1997.

[10] R. B. Marks, "A multiline method of network analyzer calibration," *IEEE Trans. Microwave Theory Tech.,* vol. 39, pp. 1205–1215, July 1991.

Simple and Efficient Computation of Electromagnetic Fields in Arbitrarily Shaped Inhomogeneous Dielectric Bodies Using Transpose-Free QMR and FFT

C. F. Wang and J. M. Jin

***Abstract*—A simple and efficient numerical method is presented for computing electromagnetic fields in three-dimensional (3-D) inhomogeneous dielectric bodies. The method employs a two-stage discretization to convert an integro–differential equation into an implicit system of linear algebraic equations. This discrete system is then solved using a transpose-free quasi-minimal residual (TFQMR) algorithm, which avoids the calculation of the multiplication between the transpose of the system matrix and a vector. The simple multiplication between the system matrix and a vector required in the TFQMR algorithm is calculated efficiently using only six fast Fourier transforms (FFT's). Numerical results for strongly inhomogenous and lossy spheres show that the method has a stable convergence behavior and excellent numerical performance.**

***Index Terms*—Electromagnetic field, fast Fourier transform, inhomogeneous dielectric bodies, transpose-free quasi-minimal residual algorithm.**

I. Introduction

Efficient computation of electromagnetic fields in arbitrarily shaped inhomogeneous dielectric bodies in a three-dimensional (3-D) space

Manuscript received January 13, 1997; revised December 5, 1997. This work was supported by the Office of Naval Research under Grant N00014-95-1-0848, by the National Science Foundation under Grant NSF ECE 94-57735, and by a grant from the Air Force Office of Scientific Research via the MURI program under Contract F49620-96-1-0025.

The authors are with the Center for Computational Electromagnetics, Department of Electrical and Computer Engineering, University of Illinois at Urbana-Champaign, Urbana, IL 61801-2991 USA.

Publisher Item Identifier S 0018-9480(98)03169-X.

0018–9480/98$10.00 © 1998 IEEE